INTERGRANULAR CORROSION MECHANISM OF ALLOY 400

William Zhang

Department of Chemical Engineering and Applied Chemistry, University of Toronto
200 College Street, Toronto, ON, M5S 3E5, Canada

The objective of this study is to find the reason for the intergranular corrosion (or intergranular attack, IGA) of Monel 400 (70Ni-30Cu) tubes that occurs occasionally in practice. Generally, the hypothesized factors of IGA for Monel 400 tubing could be crevices, dissolved oxygen, low pH, reduced sulfur species, and precipitation of impurities at grain boundaries. Electrochemical techniques including cyclic polarization and long-term potentiostatic polarization were used to test two heats of Monel 400 tubing that had behaved differently in practice. To simulate the situation within a crevice or under a deposit, cupric ions were added to the base solution, which was either neutral or acidic in pH. Artificial crevices without the addition of cupric ions in the base solution and a limiting current model were created which helped to elucidate the mechanism of IGA. The effect of thiourea as a representative reduced sulfur compound was investigated. The results show that in neutral solution IGA occurs with little sensitivity to metallurgy and does not require thiourea, but in acid solution it only occurs with thiourea addition, and particular grain boundary microstructures are more susceptible.

Key words: intergranular corrosion, crevice corrosion, Monel 400, thiourea

Introduction

Monel 400 (70Ni-30Cu) as a versatile alloy has been used for more than 100 years [1]. It has been used in a various applications, such as steam generation, heat-exchanger tubing, the refining of uranium for production of nuclear power, food processing, cladding for splash zones on offshore structures and riser pipes, and service in hydrofluoric acid and fluoride salts and caustic environments.

Pitting is uncommon for Monel 400, and the difference in standard potentials between Cu and Ni is not large enough to make de-alloying occur easily. This good performance of Monel 400 is mainly because of its composition: it combines the noble property of Cu and the passivating tendency of Ni.

Stress corrosion cracking (SCC) of Monel 400 is rare, but has occurred in oxygenated hot water, especially at sites of local cold-work [2-4]. It has also been found in slow strain rate tests in various media [5] and is susceptible to cracking in the presence of lead [6]. Like all nickel base materials, Monel is susceptible to reduced sulfur compounds, including through the interaction with sulfate-reducing bacteria [7-11]. Such behavior is consistent with the usual sensitivity of nickel to adsorbed S^0 [12] It was reported that Monel can be damaged by chemical cleaning formulations [13, 14], and this can possibly be interpreted using electrochemical kinetic studies

[15-17]. Such studies are, however, hard to interpret with regard to the possible role of de-alloying of Ni, which requires a different approach illustrated in this paper.

One concern with Monel is its susceptibility to intergranular corrosion, often called IGA, which may be the underlying mechanism of some reported cases of pitting or underdeposit attack [18-22]. In industrial plant where the redox potential fluctuates, corrosion may propagate by alternate phases of highly localized (intergranular) and more uniform dissolution.

The present work was based on the hypothesis that IGA of Monel could have an underlying de-alloying mechanism. Since copper alloys such as brass are easily de-alloyed in copper salt solutions, such as Cu^+ in NaCl or ammonia [23-26], and since practical cases of Monel corrosion often involve deposits where Cu ions can accumulate, we have used acidic and neutral $CuSO_4$ solutions and focused on the region close to the Cu equilibrium potential, where Ni can dissolve but not Cu, or at least, Cu cannot dissolve at a microstructurally significant rate. Thiourea was used in some experiments as a source of reduced sulfur. The results of these simulation experiments were compared with artificial crevice exposures, for which it was necessary to determine the diffusivity of Cu^{2+} ions in the crevice.

Experimental Procedures

Materials

Two heats of Monel 400 tubing (Ni_2B precipitates were found along the grain boundaries of one Monel which is called Monel 1, 31.5% Cu, 64.3% Ni, balanced mainly by Mn and Fe; Ni_2B precipitates were found inside the bulk solution rather than the grain boundaries of another Monel which is called Monel 2, 30.8% Cu, 65.5% Ni, balanced mainly by Mn and Fe) were acquired. These materials had behaved differently in practice, with Monel 1 showing more sensitivity to IGA.

Pure copper wire (>99.9% Cu) with a diameter of 0.17 mm was mounted in heat resistant resin as a “pencil” electrode in order to find the diffusion coefficient of Cu^{2+} which is needed for interpretation of crevice experiments on copper and Monel rods.

Pure copper rod (>99.9% Cu) and Monel rod (33.5% Cu, 63.8% Ni, balanced mainly by Mn and Fe) were machined to a diameter of 6.35 mm and were mounted in heat resistant resin for crevice corrosion studies.

Pure nickel rod (Goodfellow; <17 ppm total impurities) with the diameter of 2 mm and pure copper (>99.9%) were mounted for the anodic potentiodynamic studies.

Electrochemistry

The three-electrode electrochemical cell was a 500 ml glass vessel with a water jacket for heating and temperature control. A platinum counter electrode and saturated mercury/mercury sulfate electrode (MSE) were used for most experiments. PAR 2263A and Gamry Instruments, Reference 600 software-controlled electrochemical systems were used. In some experiments, a copper rod was used as reference electrode. Argon (Prepurified, 99.998%) was used for deoxygenation.

Initial potentiodynamic and EIS studies were done at 80°C on copper, nickel and the two Monels in 0.125M H_2SO_4 + 0.125M Na_2SO_4 with a room-temperature pH of 1.13 (pH at 80°C of 1.41). Long-term potentiostatic studies were done at potentials of 0 and 10 mV vs. Cu in a similar solution containing 0.05M $CuSO_4 \cdot 5H_2O$ with a room-temperature pH of 1.56. All experiments were done with and without the addition of 30 ppm (0.4 mM) thiourea, or sometimes other concentrations. Neutral-solution experiments were conducted in 0.25M Na_2SO_4 + 0.05M $CuSO_4$.

The equilibrium potential of pure copper in 0.25M H_2SO_4 + 0.05M $CuSO_4$ solution at 80°C was measured. After the 500 ml 0.25M Na_2SO_4 solution was heated to 80°C and deoxygenated for one hour, the insulated connecting copper wire of the "pencil" electrode was bent and the electrode was placed upward in the solution; then a potential higher than the equilibrium potential of copper measured in the presence of Cu^{2+} was applied for one hour to form a pit first and then the measured equilibrium potential was applied for half an hour to measure the limiting current.

The crevice sample was formed by combining the crevice former and the sample through elastic band. After the 500 ml 0.25M Na_2SO_4 solution was heated to 80°C and deoxygenated for one hour, 10 ml solution was withdrawn by using a syringe from the electrochemical cell and injected into the crevice and then the crevice sample was put into the cell; the sample was taken out and refilled 20 minutes later and then put back, the argon distributor was lifted up above the solution and another 20 minutes was waited to stabilize the system. An EIS measurement was conducted and if the solution resistance was repeatable then a 12-hour potentiostatic measurement followed by an EIS measurement were started; all the experiments were conducted under the equilibrium potential of copper in acidic solution in the presence of 0.05M $CuSO_4$.

Microscopy and analysis

Monel samples that were exposed in the long-term potentiostatic experiments with Cu ions added were examined by SEM and EDX, both in surface view and as polished cross-sections.

Results and Discussion

Figure 1 illustrates the potentiodynamic behavior of nickel, copper and the 'bad' and 'good' Monels (Monel 1 and Monel 2, respectively) in acid sulfate. No passivation is evident in the anodic behavior of the Monels, showing that the presence of enriched Cu hinders passivation by Ni.

The 'bad' Monel 1 shows a distinct though slow de-alloying of Ni in the potential range -0.8 to -0.4 V (MSE). Less de-alloying is evident for the 'good' Monel 2. It is not possible to tell whether this difference is associated with IGA.

The addition of 30 ppm thiourea eliminates passivity of nickel by creating an aggressive adsorbed sulfur species – probably S^0_{ads} [12] - as shown in Figure 2. There is a large IR drop in this curve; correction as shown in Figure 4 reveals that a rapid rise in current density to >150 mA/cm^2 occurs between -600 and -500 mV. Not much change is evident in the behavior of the copper or the two Monels, except that the rate of de-alloying of the 'good' Monel 2 increases. Copper shows indications of oxidation to some Cu I species, perhaps Cu_2S, and its dissolution as Cu II is slightly inhibited by the thiourea.

It is not possible to tell from these data whether there is de-alloying occurring near the Cu II dissolution potential, whether this is enhanced by thiourea, or whether any of the corrosion is intergranular.

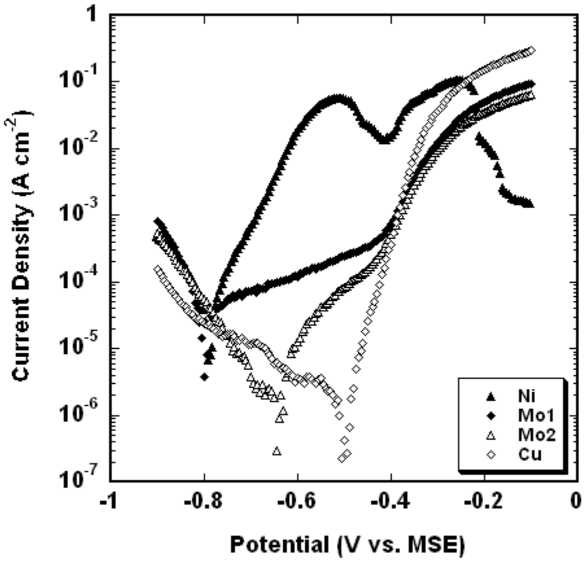

Fig.1. Anodic potentiodynamic polarization curves for Ni, Cu and two different Monels ('bad': Monel 1; 'good': Monel 2) in 0.125M H_2SO_4 + 0.125M Na_2SO_4 at 80°C. The scan rate was 5 mV/s. No IR correction has been performed.

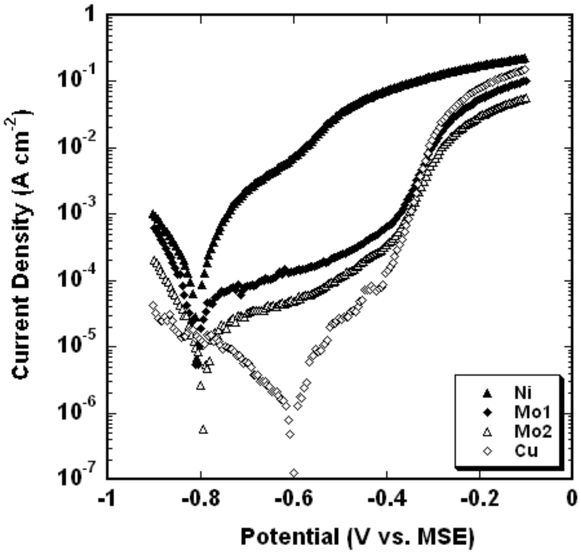

Fig.2. Anodic potentiodynamic polarization curves for Ni, Cu and two different Monels ('bad': Monel 1; 'good': Monel 2) in 0.125M H2SO4 + 0.125M Na_2SO_4 at 80°C, with 30 ppm thiourea added. The scan rate was 5 mV/s. No IR correction has been performed.

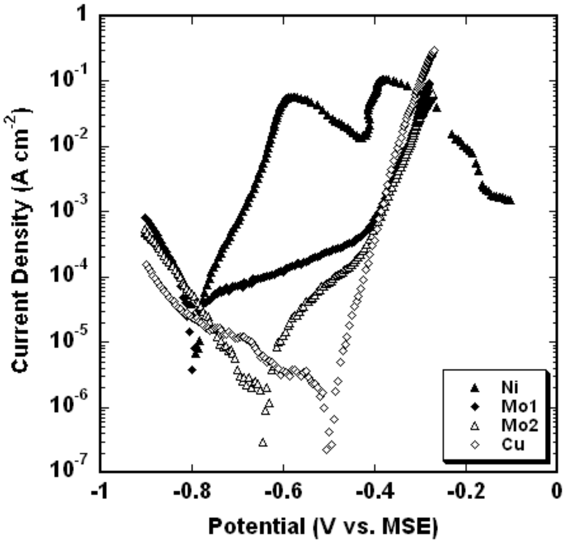

Fig.3. Same as Fig.1, with IR correction.

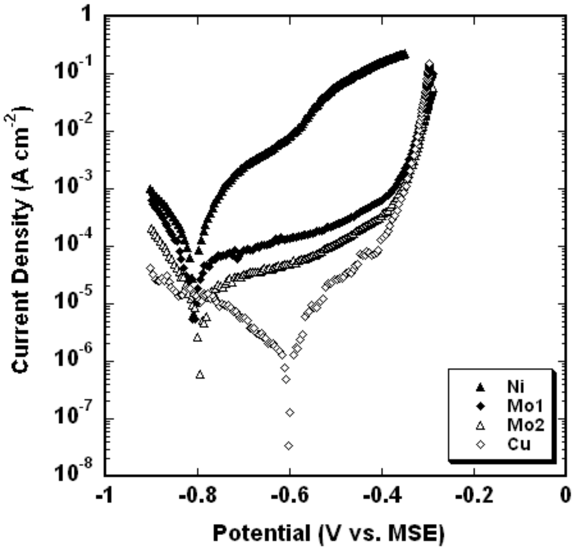

Fig.4. Same as Fig.2, with IR correction.

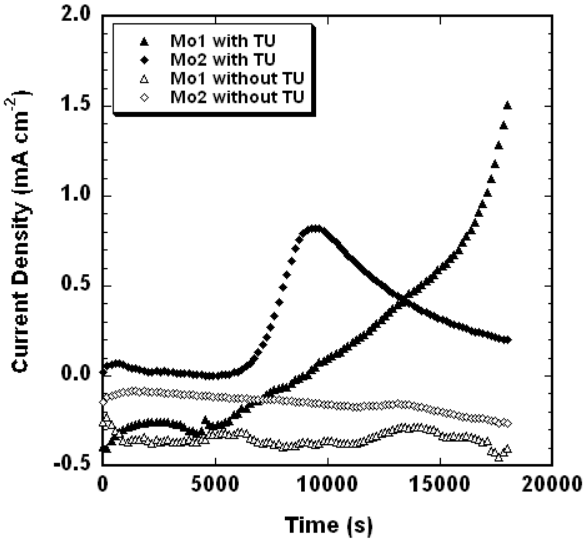

Fig.5. Current-time curves for 5-hour potentiostatic experiments on ‘bad’ and ‘good’ Monels in 0.125M H_2SO_4 + 0.125M Na_2SO_4 + 0.05M $CuSO_4$ with (a and b) and without (c and d) addition of 30 ppm thiourea, at 0 mV vs. Cu reference electrode, at 80^{o}C.

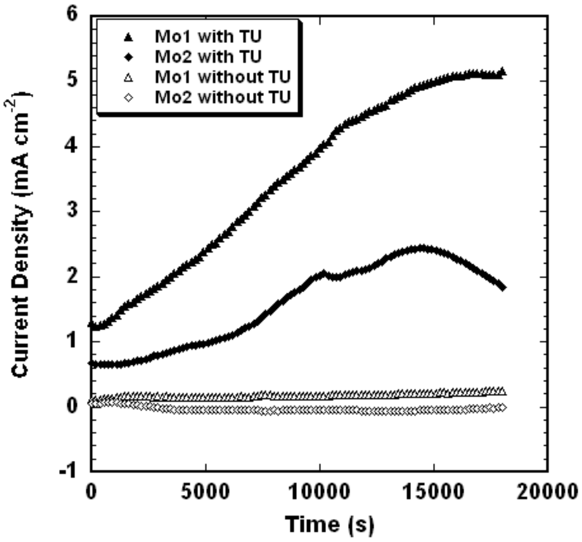

Fig.6. Current-time curves for 5-hour potentiostatic experiments on ‘bad’ and ‘good’ Monels in 0.125M H_2SO_4 + 0.125M Na_2SO_4 + 0.05M CuSO4 with (a and b) and without (c and d) addition of 30 ppm thiourea, at +10 mV vs. Cu reference electrode, at 80^{o}C.

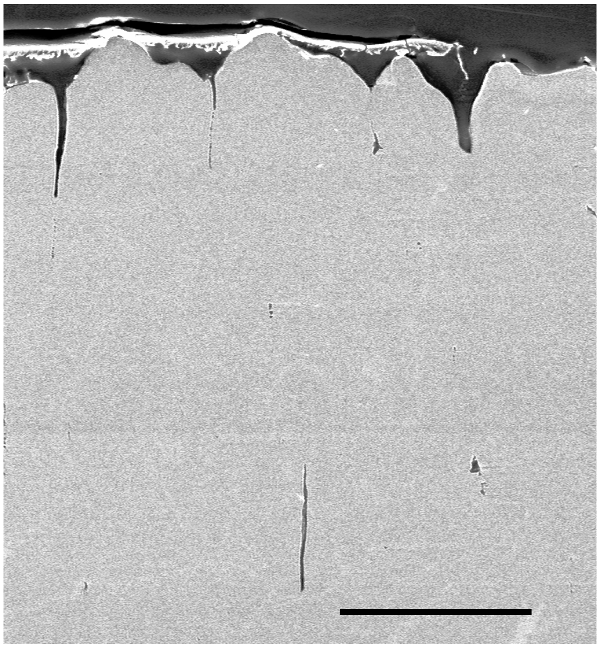

Fig.7. Cross-sectional microscopy of Mo 1 after 8-hour potentiostatic experiment on in 0.125M H_2SO_4 + 0.125M Na_2SO_4 + 0.05M $CuSO_4$ + 30 ppm thiourea, 80^oC, - 0.323 V vs. MSE, marker: 100 µm.

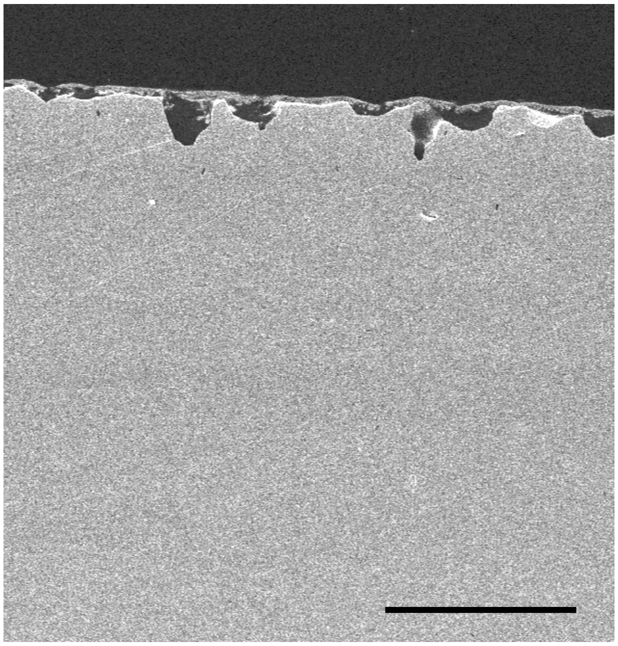

Fig.8. Cross-sectional microscopy of Mo 2 after 8-hour potentiostatic experiment in 0.125M H_2SO_4 + 0.125M Na_2SO_4 + 0.05M $CuSO_4$ + 30 ppm thiourea, 80^oC, - 0.323 V vs. MSE, marker: 100 µm.

Potentiostatic treatment near the Cu equilibrium potential in sulfate solutions with Cu II

The experiments were done with a copper reference electrode and usually lasted 5 hours in acidic solution and the experiments done with a MSE reference electrode lasted 8 hours both in acidic and neutral solutions. For acid solution at 0 mV vs. Cu, the currents are low and even cathodic without thiourea, but with thiourea there is a breakaway after about 5000 s followed by a sustained anodic current for both alloys – Figure 5. A clearer distinction between the alloys was obtained by using a potential of 10 mV vs. Cu, as shown in Figure 6: now the breakaway is earlier and the difference between the alloys is distinct. The solutions used for Figures 5 and 6 were equilibrated with Cu_2O. Much higher anodic currents were consistently obtained on the 'bad' Monel.

Figure 7 and Figure 8 show that in acidic solution in the presence of thiourea, Monel 1 suffered intergranular corrosion while the penetration of Monel 2 is very shallow, which means that IGA of Monel in acidic conditions needs the help of thiourea (or another source of recduced sulfur). Thiourea promotes corrosion by depassivating nickel through the formation of S^0_{ads}.

Reasons for heat-to-heat differences in susceptibility of Monel to IGA

In neutral solution both alloys showed IGA and it was noticed that the Cu ‘equilibrium’ potential was more positive than in acid – the Cu is actually corroding slowly to Cu_2O.
The alloys used in the present investigation have been studied by SIMS analysis of electropolished surfaces [27]. The presence of nickel boride precipitates on grain boundaries is responsible for the greater susceptibility to IGA of some Monel heats. These precipitates are essentially pure nickel, and dissolve actively, catalyzed by thiourea adsorption. Between the precipitates, nickel is removed by intergranular de-alloying.

Figure 9 and Figure 10 illustrate the potentiostatic behaviors of copper, nickel and the two Monels in neutral solution (0.25M Na_2SO_4 + 0.05M $CuSO_4$) and acidic solution (0.125M H_2SO_4 + 0.125M Na_2SO_4 + 0.05M $CuSO_4$) respectively. The applied potential used here is 10 mV vs. OCP of copper in neutral solution. In neutral solution, nickel is passivated; copper is corroded but the corrosion rate is much lower than that in acidic solution, which means the formation of Cu_2O in neutral solution blocks the further corrosion; in neutral solution the corrosion rates of the two Monels are similar and much higher than those in acidic solution.

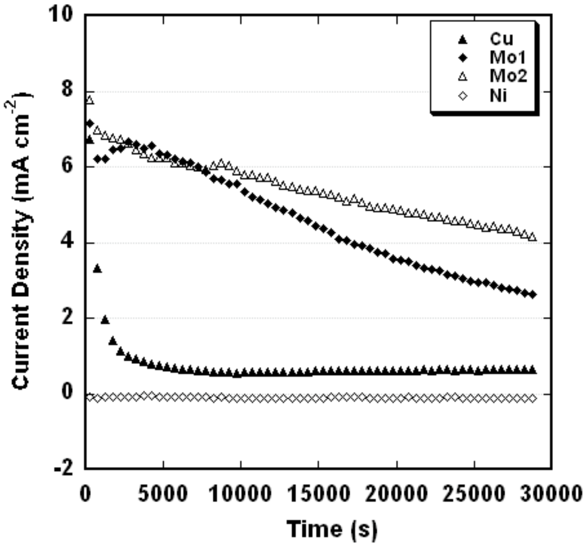

Fig.9. Current-time curves for 8-hour potentiostatic experiments on Ni, Cu and two different Monels (‘bad’: Monel 1; ‘good’: Monel 2) in 0.25M Na_2SO_4 + 0.05M $CuSO_4$ at 80^{o}C, + 10 mV vs. OCP of Cu in neutral solution.

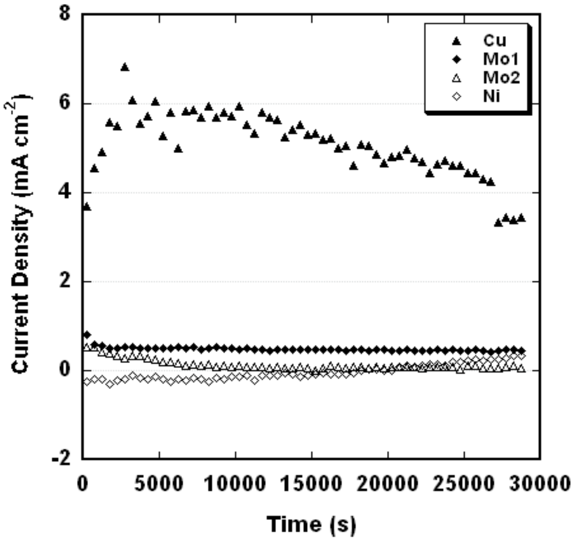

Fig.10. Current-time curves for 8-hour potentiostatic experiments on Ni, Cu and two different Monels (‘bad’: Monel 1; ‘good’: Monel 2) in 0.125M H_2SO_4 + 0.125M Na_2SO_4 + 0.05M $CuSO_4$ at 80^{o}C, + 10 mV vs. OCP of Cu in neutral solution.

Table 1 shows that in acidic solution the corrosion of Monel 1 is uniform, while with the addition of thiourea, nickel was dealloyed; nickel was dealloyed in neutral solution for both Monel 1 and Monel 2. It means that the formation of Cu_2O in neutral solution and the formation of Cu_2S in acidic solution facilitate the dealloying of nickel from Monel.

Table 1 Surface chemical compositions of Mo1 and Mo2 after being corroded (done by EDS)

	Electrolyte	Ni (atom %)	Cu (atom %)	S (atom %)
Mo1	0.125M H_2SO_4 + 0.125M Na_2SO_4 + 0.05M $CuSO_4$ + 30 ppm thiourea	5.6	84.1	10.2
Mo2	0.125M H_2SO_4 + 0.125M Na_2SO_4 + 0.05M $CuSO_4$ + 30 ppm thiourea	34.5	59.1	13.7
Mo1	0.125M H_2SO_4 + 0.125M Na_2SO_4 + 0.05M $CuSO_4$	75.7	24.3	
Mo1	0.25M Na_2SO_4 + 0.05M $CuSO_4$	13.4	86.3	
Mo1 (unattacked cross-Sectional area as a blank)	0.125M H_2SO_4 + 0.125M Na_2SO_4 + 0.05M $CuSO_4$ + 30 ppm thiourea	75.7	24.3	0.04

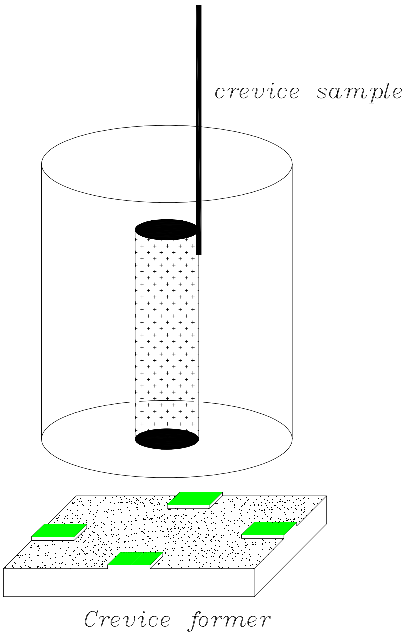

Fig.11. The fabrication of the crevice former and the working electrode

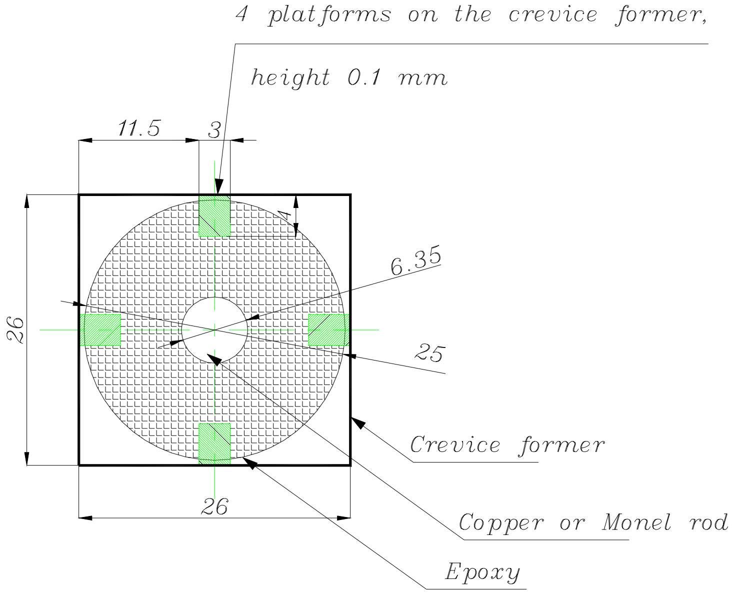

Fig.12. The dimensions of the crevice former and the working electrode

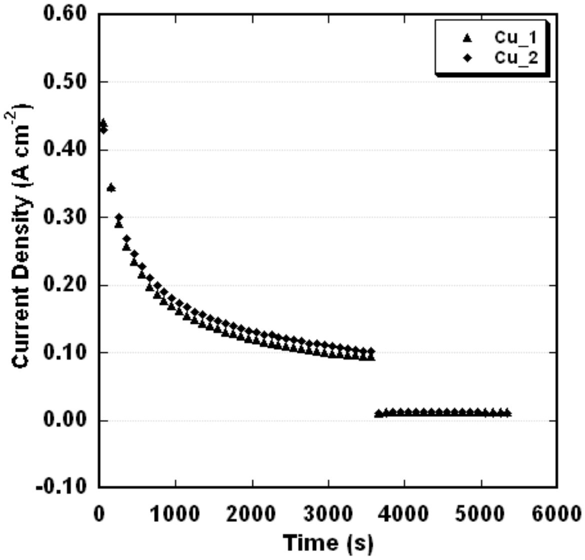

Fig.13. Potentiostatic current transient on the artificial pit corrosion, - 0.26 V vs. MSE for 1 hour, then -0.332 V vs. MSE for 0.5 hour in 0.25M Na_2SO_4 solution at 80°C

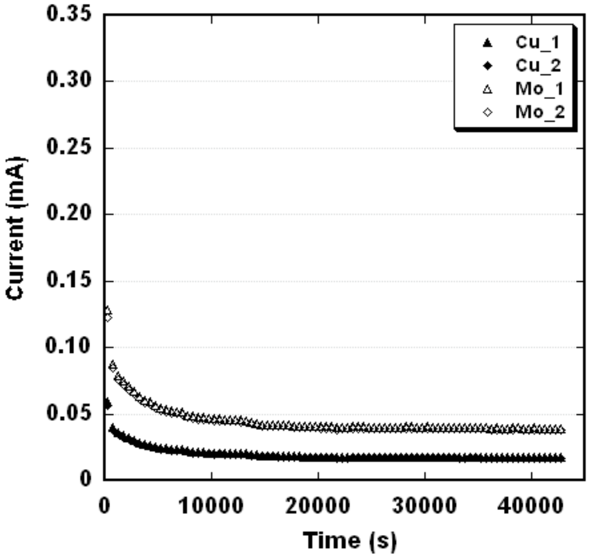

Fig.14. Current-time curves for 12-hour potentiostatic experiments on Cu rod and Monel rod crevice specimens in 0.25M Na_2SO_4 solution at -0.332 V vs. MSE and 80°C.

Crevice corrosion experiments

The fabrication of the crevice device and creviced working electrode are shown in Figures 11 and 12. The crevice height was 0.1 mm.

First we need to determine the diffusion coefficient of Cu^{2+} - we do that with the artificial pit technique as shown in Figure 13, the diffusion coefficient of Cu^{2+} was obtained as follows: the equilibrium potential of Cu^{2+}/Cu at 80°C was measured in 0.25M Na_2SO_4 + 0.05M $CuSO_4$ solution; the measured value was - 0.332 V vs. MSE. If we polarize the artificial pit at this potential without Cu^{2+} in solution, the equilibrium concentration of Cu^{2+} ions will be established at the bottom of the pit, so we will know "C_0" in the diffusion problem, thus we can determine D, as shown in Equation (1); the depth of the pit in Equation (1) can be obtained by using Equation (2); the concentration of Cu^{2+} in Equation (1) is before IR correction, the real concentration of Cu^{2+} can be obtained by using Equation (3) (Nernst Equation) and the corrected diffusion coefficient of Cu^{2+} is obtained. All this is valid because we have a relatively dilute solution in the artificial pit or crevice, in contrast to experiments where we saturate Cu^{2+} at the bottom, where the effective diffusivity will be much lower.

$$D = \frac{i_L h}{nFC_o} \qquad (1)$$

i_L – Limiting current density controlled by diffusion, A cm^{-2}
D – Diffusion coefficient, cm^2 s^{-1},
F – Faraday constant, 96500 coulombs mol^{-1},
C_o – Interfacial solution concentration, and C_o=0.05M when -0.332 V vs. MSE was applied (assuming no IR drop).

h – Depth of pit, cm

$$h = \frac{qm}{nF\rho A} \qquad (2)$$

q – Integrated charge of the artificial pit experiment, coulombs, C cm^{-2}
m – Mole weight of Cu, 63.5 g mol^{-1}
n – Valence of Cu^{2+}, 2
ρ – Density of Cu, 8.94 g cm^{-3}.

$$E = E^{o} + (2.303RT/2F)\log(\gamma \times [Cu^{2+}]) \qquad (3)$$

E – Equilibrium potential of Cu^{2+}/Cu electrode,
E^{o} – Standard equilibrium potential of Cu^{2+}/Cu electrode at 80°C,
γ – Activity coefficient of Cu^{2+}, at very low concentration, γ can be treated as a constant and this can be verified from the OLI calculation.
R – Ideal gas constant, 8.314 J/ (mol.K),
T – Temperature, K.

The diffusion coefficient of Cu^{2+} in neutral solution is 3.965x10^{-5} cm^{2}s^{-1}.

The limiting current of the Cu crevice corrosion is calculated as follows:

$$J = -D\frac{dC}{dr}, \qquad (4)$$

Where,
J – Flux, mol cm^{-2} s^{-1},
D – Diffusion coefficient, cm^2 s^{-1},
C – Concentration of Cu^{2+},
r – Radius of the sample

So the limiting current will be the flux of Cu^{2+} times the valence of Cu^{2+}, the Faraday constant and the area of the circular gap perpendicular to the flux direction, i.e.

$$I = J \cdot nF \cdot 2\pi \cdot rh = -nFD \cdot 2\pi \cdot rh\frac{dC}{dr} \qquad (5)$$

After integration,

$$I = (2\pi nFDh) \cdot C_{r=r_1} \cdot (\ln\frac{r_2}{r_1})^{-1}, \qquad (6)$$

Substitute the diffusion coefficient into Equation (6), the theoretical limiting current of copper rod crevice corrosion is as follows:

$$I = (2 \times 3.14 \times 2 \times 96500 \times 3.965 \times 10^{-5} \times 0.01) \times 0.05 \times 10^{-3} \times \ln(1.25/0.3175) = 17.54 \times 10^{-6}(A)$$
$$= 17.54(\mu A)$$

Compared this with Table 2, the obtained limiting currents of copper crevice corrosion are reasonable. The limiting current of copper crevice is used to calibrate the limiting current of Monel rod crevice corrosion, that is, according to the Nernst Equation, the corrosion potential is mainly determined by the more noble element which is copper here, by keeping the equilibrium potential of copper in 0.25M Na_2SO_4 + 0.05M $CuSO_4$ solution as the applied potential of copper in 0.25M Na_2SO_4, the concentration of Cu^{2+} at the edge of the copper electrode is 0.05M; if there is no IR drop; and same Cu^{2+} concentration will be obtained for Monel rod crevice corrosion, the rest of the current is contributed by Ni^{2+}, if the limiting current ratio of Monel rod to copper rod is equal to the ratio of the mole content of nickel and copper to that of copper, the corrosion is uniform corrosion; if the ratio is bigger than that then nickel is dealloyed; otherwise nickel is passivated. We also have to consider IR drop, and the real Cu^{2+} concentration at the edge of the electrode is corrected by applying Nernst Equation.

Table 2 Limiting current and solution resistance of crevice corrosion for copper and Monel rod

Material	Limiting current (μA)	Solution Resistance (ohm), after potentiostatic measurements
Cu rod	17.3	577
	16.7	565
Monel rod	39.2	541
	38.1	555

From the Nernst Equation and the IR drop of the Cu crevice corrosion we can find the concentration of Cu^{2+} at the edge of the working electrode as follows:

At 80°C, $E = E^o + 35\log(\gamma \times [Cu^{2+}])$ (mV)
For Cu crevice corrosion,

$$IR = (17.3 + 16.7)/(2 \times 1000) \times (577 + 565)/2 = 9.7(mV)$$

$$35\log(\gamma_1 \times [Cu^{2+}]) - 35\log(0.05 \times \gamma_2) = -9.7(mV)$$

$$\log(\tfrac{\gamma_1 \times [Cu^{2+}]}{\gamma_2 \times 0.05}) = -0.277$$

At very low concentration, γ can be treated as a constant which means $\gamma_1 = \gamma_2$, and this can be verified from the OLI calculation. So that:
$[Cu^{2+}] = 0.528 \times 0.05$

For Monel crevice corrosion,

$$IR = (39.2 + 38.1)/(2 \times 1000) \times (541 + 555)/2 = 21.2(mV)$$

$[Cu^{2+}] = 0.248 \times 0.05$,
If there is no selective dissolution of nickel in Monel, the current ratio should be as follows:

$$\frac{I_{Monel}}{I_{Cu}} = \frac{3 \times 0.248}{0.528} = 1.41$$

The current ratio obtained from experiment is as follows:
$(39.2+38.1)/(17.3+16.7)=2.27>1.41$
This confirms that nickel was being dealloyed in the crevice corrosion. Analytical confirmation will be presented elsewhere.

Conclusions

1. IGA of Monel in acidic conditions needs the help of thiourea (or another source of recduced sulfur). Thiourea promotes corrosion by depassivating nickel through the formation of S^0_{ads}. The mechanism of this corrosion involves de-alloying of nickel and is facilitated by active dissolution of nickel boride precipitates at the grain boundaries.

2. The formation of Cu_2O on the Monel surface plays a role in neutral solution – it reduces the surface mobility of Cu atoms and facilitates the local dissolution of nickel from Monel.

3. The formation of Cu_2S in acidic solution with thiourea may play a similar role– facilitating the dealloying of nickel by reducing the surface diffusion of Cu atoms.

4. The current ratio (2.27) obtained from crevice experiments in neutral solution is much bigger than that from the model calculation (1.41), which means that there is a selective dissolution of nickel, which is compatible with the experimental results obtained from the bulk solution method.

Acknowledgements

This research was supported by NSERC (Canada) and by UNENE, the University Network of Excellence in Nuclear Engineering.

References

1. S. E. Lewis and G.D. Smith, a Century of Monel Metel: 1906-2006, JOM. vol. 58, no 9, pp 22-26, Sept. 2006.
2. S. Sato and K. Nagata, Sumitomo Light Metal Tech. Rep., vol 15, no 4, pp 40-57, Oct. 1974.
3. J.A. Beavers, A.K. Agrawal and W.E. Berry, J. Mater. Energy Syst., vol 4, pp 168-181 (1982).
4. J.A. Beavers, A.K. Agrawal, W.E. Berry and B.C. Syrett, Corrosion/84, paper #169, NACE, Houston (1984).
5. L.G. Everhart and C.E. Price, Stress corrosion cracking in Alloy 400 at room temperature, in Corrosion Testing and Evaluation: Silver Anniversary Volume, pp 319-334, ASTM STP 1000 (1990).

6. M.D. Wright, G. Goszczynski and F. Peca, Embrittlement of Alloy 400 by lead in secondary side steam generator environments, in Proc 7th Int. Symp. Environmental Degradation of Materials in Nuclear Power Systems – Water Reactors, pp 209-217, NACE, Houston (1995).
7. R.A. Buchanan, A.L. Kovacs, C.D. Lundin, K.K. Khan, J.C. Danko, P. Angell and S.C. Dexter, Corrosion/96, paper #274, NACE, Houston (1996).
8. V.K. Gouda, I.M. Banat, W.T. Riad and S. Mansour, Corrosion, vol 49, pp. 63-73 (1993).
9. J.M. Popplewell, Corrosion/80, paper #180, NACE, Houston (1980).
10. M. Valliappan, M. Natesan, G. Venkatachari and K. Balakrishnan, Bull. Electrochem., vol 6, pp 213-214 (1990).
11. B. Little, P. Wagner, R. Ray and J.M. Jones, Corrosion/91, paper #101, NACE, Houston (1991).
12. P. Marcus, Corrosion Mechanisms in Theory and Practice, 2nd edition, pp 287-310, ed. P. Marcus, Marcel Dekker, New York (2002).
13. S. Padma, S. N. Veena, A. L. Rufus, V. S. Sathyaseelan, S. Velmurugan, S. V. Narasimhan, Materials and Corrosion, vol 52, pp 771-780 (2001).
14. R. Latha, S. Rangarajan, S.V. Narasimhan, S. Rajeswari and M. Subbaiyan, Proc CORCON-97: Corrosion and Its Control. II (Mumbai, 1997), pp 1224-1230, Elsevier, Amsterdam (1998).
15. P.K. De and A. Bose, Corrosion, vol 49, pp 135-145 (1993).
16. J.A. Ali and J.R. Ambrose, Corros. Sci., vol 33, pp 1147-1159 (1992).
17. J.A. Ali and J.R. Ambrose, Corros. Sci., vol 32, pp 799-814 (1991).
18. P.J. King and D.P. Dautovich, Nucl. Technol., vol. 55, pp 196-206 (1981).
19. J.T. Francis, N.S. McIntyre, R.D. Davidson, S. Ramamurthy, A.M. Brennenstuhl, A. McBride and A. Roberts, Surface and Interface Analysis, vol 33, pp 29-34 (2002).
20. J.T. Francis, A.M. Brennenstuhl, S. Ramamurthy and N.S. McIntyre, Surface and Interface Analysis, vol 34, pp 189-191 (2002).
21. N.S. McIntyre, R.D. Davidson, T.L. Walzak and A.M. Brennenstuhl, Corros. Sci., vol 37, pp 1059-1083 (1995).
22. N.G. Muralidharan, N. Raghu, K.V. Kasiviswanathan, T. Jayakumar and B. Raj, Proc CORCON-97: Corrosion and Its Control. II (Mumbai, 1997), pp 946-951, Elsevier, Amsterdam (1998).
23. R.C. Newman, T. Shahrabi and K. Sieradzki, Corros. Sci., vol 28, pp 873-886 (1988).
24. R.C. Newman and T. Shahrabi, Corrosion, vol 49, pp 60-62 (1993).
25. T. Shahrabi, R.C. Newman and K. Sieradzki, J. Electrochem. Soc., vol 140, pp 348-352 (1993).
26. K. Sieradzki, J.S. Kim, A.T. Cole and R.C. Newman, J. Electrochem. Soc., vol 134, pp 1635-1639 (1987).
27. A. Brennenstuhl, OPG, personal communication.